# Divergent roles of IREG/Ferroportin transporters from the nickel hyperaccumulator *Leucocroton havanensis*

Dubiel Alfonso Gonzalez[1,2*], Vanesa Sanchez Garcia de la Torre[3], Rolando Reyes Fernandez[2], Louise Barreau[3], Sylvain Merlot[3,4*]

[1] *Jardín Botánico Nacional, Universidad de La Habana, Carretera "El Rocío" km 3.5, Calabazar, Boyeros, La Habana, Cuba.*

[2] *Universidad Agraria de La Habana, Facultad de Agronomía, Autopista Nacional Km 23 ½, 32700, San José de las Lajas, Mayabeque, Cuba.*

[3] *Université Paris-Saclay, CEA, CNRS, Institute for Integrative Biology of the Cell (I2BC), 91198, Gif-sur-Yvette, France.*

[4] *Laboratoire de Recherche en Sciences Végétales (LRSV), UMR5546 CNRS/UPS/INPT, 31320, Auzeville- Tolosane, France.*

[*] For correspondence: dubiel.alfonso@gmail.com; sylvain.merlot@univ-tlse3.fr

1 **Highlight**

2 The nickel hyperaccumulator *Leucocroton havanensis* endemic to Cuba, expresses two

3 paralogous metal transporters of the IREG/ferroportin family that play distinct but

4 complementary roles in nickel tolerance and accumulation.

5

6 **Abstract**

7

8 In response to our ever-increasing demand for metals, phytotechnologies are being developed

9 to limit the environmental impact of conventional metal mining. However, the development of

10 these technologies, which rely on plant species able to tolerate and accumulate metals, is partly

11 limited by our lack of knowledge of the underlying molecular mechanisms.

12 In this work, we aimed to identify genes involved in nickel hyperaccumulation in the

13 Euphorbiaceae species *Leucocroton havanensis*. Using transcriptomic data, we identified two

14 homologous genes, *LhavIREG1* and *LhavIREG2*, encoding divalent metal transporters of the

15 IREG/ferroportin family. Both genes are expressed at similar levels in shoots, but LhavIREG1

16 shows higher expression in roots. Heterologous expression of these transporters in *A. thaliana*

17 revealed that LhavIREG1 is localized to the plasma membrane, whereas LhavIREG2 is located

18 at the vacuole. In addition, expression of each gene induced a significant increase in nickel

19 tolerance. Taken together, our data suggest that LhavIREG2 is involved in nickel sequestration

20 in vacuoles of leaf cells, whereas LhavIREG1 is mainly involved in nickel translocation from

21 roots to shoots, but could also be involved in metal sequestration in cell walls. Our results

22 suggest that paralogous IREG/ferroportin transporters may play complementary roles in nickel

23 hyperaccumulation in plants.

24

**Introduction**

25

26 Since the beginning of the industrial revolution, and today accelerated by the energy transition

27 required to reduce $CO_2$ emissions, metal use intensity is increasing exponentially for strategic

28 metals. Metal mining and refining are responsible for the dispersion of metals from primary

29 sites, increasing the risk of contamination in the natural environment and agricultural soils

30 (Dudka and Adriano, 1997; Li *et al.*, 2014; Sonter *et al.*, 2020; Vidal *et al.*, 2022).

31 Phytotechnologies based on plants capable of hyperaccumulating metals have been proposed

32 as a solution to limit the environmental impact of metal mining, remediate contaminated soils

33 and recycle valuable metals (Suman *et al.*, 2018; DalCorso *et al.*, 2019; Corzo Remigio *et al.*,

34 2020). The development of these phytotechnologies is particularly relevant in Mediterranean

35 and tropical regions where nickel mining can have a significant impact on rich biodiversity (van

36 der Ent *et al.*, 2015). As for other crops, a better understanding of the molecular mechanisms

37 involved in metal tolerance and accumulation will support the development of sustainable

38 phytotechnologies using hyperaccumulators.

39 Metal hyperaccumulators are plant species that are able to tolerate and accumulate enormous

40 amounts of metal in their leaves (van der Ent *et al.*, 2013). More than 700 hyperaccumulators

41 have been identified, accumulating a wide variety of metals such as nickel, zinc or manganese.

42 However, nickel hyperaccumulators represent the vast majority of these species (Reeves *et al.*,

43 2018). At the molecular level, metal hyperaccumulation requires high activity of genes involved

44 in metal chelation and transport, from metal uptake by roots to metal storage in leaves (Manara

45 *et al.*, 2020). Accordingly, molecular studies, mostly performed in hyperaccumulators from the

46 Brassicaceae family, suggest that metal hyperaccumulation has evolved from the high and

47 constitutive expression of genes involved in the regulation of metal homeostasis in plants

48 (Becher *et al.*, 2004; Weber *et al.*, 2004; Hammond *et al.*, 2006; Halimaa *et al.*, 2014). For

49    example, zinc hyperaccumulation in *Arabidopsis halleri* has evolved from the triplication of

50    the *heavy metal Atpase 4* (*AhHMA4*) gene and mutations in cis-elements leading to high

51    expression of this metal pump. The high activity of *AhHMA4* promotes zinc loading in the

52    xylem and thus efficient translocation of zinc to the shoots (Hanikenne *et al.*, 2008).

53    Interestingly, similar genetic mechanisms are proposed to be at the origin of zinc

54    hyperaccumulation in *Noccaea caerulescens*, suggesting that the high expression of *HMA4* is

55    a convergent mechanism involved in zinc hyperaccumulation in Brassicaceae (Ó Lochlainn *et*

56    *al.*, 2011; Craciun *et al.*, 2012). Recent studies have shown that the high expression of divalent

57    metal ion transporters of the IREG/ferroportin family (IREG/FPN) is repeatedly associated with

58    nickel hyperaccumulation in several plant families (Merlot *et al.*, 2014; Halimaa *et al.*, 2014;

59    Meier *et al.*, 2018; García de la Torre *et al.*, 2021).

60    Plant genomes contain two distinct groups of IREG/FPN transporters (Schaaf *et al.*, 2006;

61    Taniguchi *et al.*, 2015; García de la Torre *et al.*, 2021). The first group, represented by

62    *Arabidopsis thaliana* AtIREG3/MAR1, encodes plastid transporters that are likely involved in

63    the regulation of iron homeostasis in chloroplasts and mitochondria (Conte *et al.*, 2009; Kim *et*

64    *al.*, 2021). The second group, represented by AtIREG1/FPN1 and AtIREG2/FPN2 in *A.*

65    *thaliana*, encodes vacuolar and plasma membrane transporters (Morrissey *et al.*, 2009).

66    AtIREG2/FPN2 was shown to be expressed in roots in response to iron starvation and localized

67    to the vacuolar membrane. The *A. thaliana ireg2* mutant is more sensitive to nickel, suggesting

68    that AtIREG2 transports nickel into vacuoles to limit metal toxicity. Accordingly, plants

69    overexpressing *AtIREG2* are more resistant to nickel and accumulate more of this metal (Schaaf

70    *et al.*, 2006). In contrast, AtIREG1/FPN1 localizes to the plasma membrane and has been

71    proposed to mediate the loading of cobalt into the xylem for long-distance transport to the shoot

72    (Morrissey *et al.*, 2009). However, the *ireg1* mutation further increases the nickel sensitivity

73    associated with *ireg2*, suggesting that AtIREG1 is also capable of transporting nickel. Analysis

74    of orthologous transporters from *Medicago truncatula* (MtFPN2) and from *rice* (OsFPN1)

75    revealed that group 2 IREG/FPN transporters can also be found in endomembranes and Golgi

76    respectively (Escudero *et al.*, 2020; Kan *et al.*, 2022).

77    To date, functional analyses of cellular IREG/FPN transporters associated with nickel

78    hyperaccumulation have suggested that these transporters are involved in the storage of nickel

79    in the vacuole of leaf cells (Merlot *et al.*, 2014; García de la Torre *et al.*, 2021). However, the

80    genomes of several nickel hyperaccumulators contain more than one gene encoding for group

81    2 IREG/FPN transporters. Interestingly, the nickel hyperaccumulator *Leucocroton* havanensis,

82    endemic to Cuba, expresses two genes coding for group 2 IREG/FPN transporters in leaves,

83    whereas the related nonaccumulator species *Leucocroton havanensis* apparently expresses only

84    one gene (Jestrow *et al.*, 2012; García de la Torre *et al.*, 2021). This observation raises the

85    question of the role of homologous group 2 IREG/FPN transporters in nickel

86    hyperaccumulation.

87    In this work, we have studied the function of the two group 2 IREG/FPN transporters,

88    LhavIREG1 and LhavIREG2, identified in the nickel hyperaccumulator *Leucocroton*

89    *havanensis*. Our results indicate that the two genes have distinct expression patterns in roots

90    and shoots and localize to different cellular membranes. Heterologous expression in *A. thaliana*

91    further suggestss that the two genes have different functions in nickel transport and may

92    therefore play distinct but complementary roles in nickel tolerance and accumulation.

93

94

5

**Materials and Methods**

*Leucocroton havanensis plant material*

*Leucocroton havanensis* seeds were collected from a single female specimen (23°04'55.5"N 82°06'46.1"W) growing on ultramafic soil in the ecological reserve "La Coca" (Havana, Cuba). Seeds and young plantlets were grown *in vitro* on Murashige and Skoog agar medium supplemented or not with 3.2 mM $NiSO_4$ for 6 weeks after germination as previously described (González and Matrella, 2013). Root and shoot samples were collected separately and washed with distilled water. After rapidly removing water with a paper towel, samples were cut into 3 mm pieces and immediately placed in RNAlater (Sigma-Aldrich). Samples were transported from Cuba to France and stored at -80°C until processing.

*Transcriptomic analyses*

RNA from *L. havanensis* root and leaf samples treated or not with nickel were extracted using Tri reagent (Sigma-Aldrich). RNA sequencing, *de novo* transcriptome assembly, transcriptome annotation, read mapping and differential gene expression analysis were performed essentially as described previously (García de la Torre *et al.*, 2021). The *de novo* assembly of the transcriptome (Lhav_v2), was performed using RNA-seq reads from root and shoot samples of nickel-treated plantlets. The quality of the assembly was analyzed by the TransRate v1.0.3 package using the trimmed read sequences used to assemble Lhav_v2 (Smith-Unna *et al.*, 2016). The completeness of the assembled transcriptome was estimated using BUSCO (v 4.0.6) and viridiplantae_odb10 lineage dataset (Seppey *et al.*, 2019). Differential gene expression analysis was performed using the edgeR bioconductor package with TMM normalization and Exact test for statistical analysis, with one repetition per sample. Genes with absolute fold change $|FC| \geq 10$ and adjusted p-value $\leq 0.05$ were considered as differentially expressed (DE) genes.

6

120

### *Reconstruction and cloning of LhavIREG coding sequences*

122  The coding sequence of *LhavIREG1* was predicted from transcriptome Lhav_v2 contigs #981

123  and #4486, and from transcriptome Lhav_v1 contigs #820 and #4646. The coding sequence of

124  *LhavIREG2* was predicted from transcriptome Lhav_v2 contig #101 and from transcriptome

125  Lhav_v1 contigs #170 and #14018. The coding sequence of *LhavIREG3* was predicted from

126  transcriptome Lhav_v2 contigs #6824 and #12273, and from transcriptome Lhav_v1 contigs

127  #8277, #9347 and #4646.

128  The coding sequences of *LhavIREG1* and *LhavIREG2* were amplified from leaf cDNA using

129  high-fidelity Phusion polymerase (Thermo Scientific) with gene-specific primers containing

130  the attB recombination sequences attB1_LhavIREG1_For*/*attB2_LhavIREG1_Rev-(no)stop

131  and attB1_LhavIREG2_For*/*attB2_LhavIREG2_Rev-(no)stop respectively (Table S1). The

132  PCR products were recombined into pDONOR207 using GATEWAY technology (Invitrogen)

133  to generate pDON207-*LhavIREG1(no)stop* and pDON207-*LhavIREG2(no)stop*. We confirmed

134  the predicted sequences of the *LhavIREG1* and *LhavIREG2* coding regions by double-strand

135  Sanger sequencing (GATC-Eurofins).

136

### *Phylogenetic analysis*

138  Sequences for IREG/FPN proteins were obtained from Dicots Plaza 5.0 (Van Bel *et al.*, 2022),

139  for *Arabidopsis thaliana* AthaIREG1 (AT5G03570), AthaIREG2 (AT2G38460), AthaIREG3

140  (AT5G26820); *Arabidopsis lyrata* AlyrIREG1 (AL4G35730), AlyrIREG2 (AL6G13070),

141  AlyrIREG3 (AL6G38700); *Eutrema salsugineum* EsalIREG1 (Thhalv10013299m.g),

142  EsalIREG2 (Thhalv10016525m.g), EsalIREG3 (Thhalv10003867m.g); *Teobroma cacao*

143  TcacIREG1 (Thecc.05G005200), TcacIREG2 (Thecc.05G005300), TcacIREG3

144  (Thecc.05G323900); *Cucumis melo* CmelIREG1 (MELO3C026034.2), CmelIREG3

145 (MELO3C004177.2); *Phaseolus vulgaris* PvulIREG1 (Phvul.010G062200), PvulIREG2

146 (Phvul.010G062300), PvulIREG3 (Phvul.007G201800); *Nicotiana tabacum* NtabIREG1

147 (Nitab4.5_0000355g0170), NtabIREG2 (Nitab4.5_0012987g0010), NtabIREG3_1

148 (Nitab4.5_0001338g0110), NtabIREG3_2 (Nitab4.5_0004525g0030); *Chenopodium quinoa*

149 CquiIREG1 (AUR62006302), CquiIREG2 (AUR62026347), CquiIREG3_1 (AUR62000385),

150 CquiIREG3_2 (AUR62006741) and *Erigeron canadensis* EcanIREG1 (ECA247G0592). The

151 sequences of *Ricinus communis* RcomIREG1 (XP_048225718.1), RcomIREG2

152 (XP_048235846.1), RcomIREG3 (XP_002512519.1) and *Homo sapiens* HsapFPN

153 (XP_047300022.1) were obtained from NCBI. The sequences of *Leucocroton havanensis*

154 LhavIREG1, LhavIREG2 proteins were translated from the corresponding cDNA sequences

155 (OR234317, OR234318). The sequence of LhavIREG3 was deduced from the corresponding

156 contigs. Protein alignment was performed with CLC Genomics Workbench 22.0.1 (Qiagen)

157 using MUSCLE v3.8.425 (Edgar, 2004). The tree was constructed using maximum likelihood

158 phylogeny (neighbor-joining, 100 bootstrap replicates) and displayed using iTol v6 (Letunic

159 and Bork, 2021).

160

161 ***Quantification of gene expression by RT-qPCR***

162 Total RNA was extracted with TRI reagent according to the manufacturer's instructions

163 (Sigma-Aldrich) and purified with RNeasy Plant Mini Kit on-column DNase I treatment

164 (Qiagen). cDNA synthesis, quantitative PCR amplification and analysis were performed as

165 previously described (García de la Torre *et al.*, 2021). The expression of *LhavIREG1* and

166 *LhavIREG2* was normalized to the expression of the *histidine kinase 3* gene (*LhavH3K*;

167 Lhav_v2 contig #1232), which was chosen as a reference because of its stable expression in

168 our transcriptomic data. Primers used for RT-qPCR experiments are given in Table S1. The

169 relative expression of *LhavIREG1* and *LhavIREG2* was quantified according to Pfaffl (2001).

170

*Analysis of LhavIREG1 and LhavIREG2 activity in yeast*

pDON207-*LhavIREG1stop* and pDON207-*LhavIREG2stop* were recombined with pDR195-GTW (Oomen *et al.*, 2009) to generate pDR195-*LhavIREG1* and pDR195-*LhIREG2*. These constructs were transformed together with pDR195-GTW and pDR195-*AtIREG2* (Schaaf *et al.*, 2006) into *Saccharomyces cerevisiae* strain Y00000H strain (BY4741; *MAT*a; *leu2Δ*; *met15Δ*; *ura3Δ*). Nickel accumulation in yeast was essentially determined as previously described (Merlot *et al.*, 2014; García de la Torre *et al.*, 2021). Yeast cells were grown in 50 ml of liquid SD-Ura medium supplemented with 400 µM $NiCl_2$ for 30 h at 28 °C with vigorous shaking. Cells were harvested by centrifugation at 4 °C and pellets were washed twice with ice-cold [10 mM EDTA, 20 mM MES pH 5.5] and once with ice-cold ultrapure water. Yeast pellets were dried at 65°C prior to elemental analysis.

182

*Expression of LhavIREG1* **and** *LhavIREG2* **in** *Arabidopsis thaliana*

pDON207-*LhavIREG1nostop* and pDON207-*LhavIREG2nostop* were recombined with the plant expression vector pMUBI83 (Merlot *et al.*, 2014) to express C-terminal protein fusions with the green fluorescent protein (GFP). Both constructs pMUBI83-*LhavIREG1* and pMUBI83-*LhIREG2* were transformed into the *A. thaliana ireg2-1* mutant (Schaaf *et al.*, 2006) as described previously (Merlot *et al.*, 2014). For each construct, three homozygous, single locus insertion, T3 lines, expressing the fluorescent protein were selected. T3 lines together with *ireg2-1* and WT (Col) were grown *in vitro* for 10 days on Hoagland agar medium containing 10 µM Fe-HBED and supplemented with 30 or 50 µM $NiCl_2$. Primary root length was measured as described previously (Merlot *et al.*, 2014). To measure metal accumulation, plants were grown on Hoagland agar medium containing 10 µM Fe-HBED for 7 days and then

194    transferred to the same medium supplemented with 50 µM $NiCl_2$ for 5 days. Roots and shoots

195    samples were prepared for elemental analyses as previously described  (Merlot *et al.*, 2014).

196

197    *Quantitative elemental analyses*

198    The dry weight of yeast and plant samples was measured before mineralization in 2 ml of 70%

199    $HNO_3$ for 4 h at 120 °C. Samples were diluted with ultrapure water to a total volume of 12 ml,

200    and metal content was measured using a 4200 MP-AES spectrophotometer (Agilent

201    technologies) as previously described (García de la Torre *et al.*, 2021).

202

203    *Confocal imaging*

204    Roots of *ireg2-1* transgenic T2 lines transformed with pMUBI83-*LhavIREG1* and pMUBI83-

205    *LhavIREG2* were imaged on a Leica SP8X inverted confocal microscope (IMAGERIE-Gif

206    platform www.i2bc.paris-saclay.fr/bioimaging/) as previously described (Merlot et al. 2014),

207    with laser excitation at 490 nm and collection of emitted light at 500-550nm for GFP and

208    600-650 nm for propidium iodide.

209

210    *Statistics*

211    GraphPad (v7.05) and the shiny application SuperPlotsOfData (Lord *et al.*, 2020) were used

212    for ttatistical analyses and data presentation.

213

## Results

**Analysis of leaf and root transcriptomes of *Leucocroton havanensis***

In a previous study, we generated the leaf transcriptome of *Leucocroton havanensis* (Lhav_v1) and compared it with the leaf transcriptome of the related nonaccumulator species *Lasiocroton microphyllus* to identify genes associated with the nickel hyperaccumulation trait (García de la Torre *et al.*, 2021). In this study, we wanted to deepen our knowledge of the root and shoot mechanisms involved in nickel hyperaccumulation in *L. havanensis*. We sequenced RNA from roots and shoots to generate a new transcriptome assembly for this nickel hyperaccumulator species (Lhav_v2). This assembly consists of 65936 contigs with 14320 contigs larger than 1kb (Table 1). 31936 contigs (48%) were annotated with Blast2GO and 12771 contigs (19%) with Mercator 4. We then used this transcriptome as a reference to analyze the effect of nickel on gene expression in *L. havanensis* (Figure 1, Table S2). We identified 27 contigs differentially expressed (DE) in response to nickel in roots (Figure 1B), indicating a limited effect of nickel hyperaccumulation on gene expression in this tissue. Among the 19 contigs up-regulated in response to nickel in roots, contigs encoding for seed storage proteins (MapMan4 category 19.5.1) are overrepresented (4 contigs, FDR adj. p-value = 3.1e-07). In contrast, we identified 442 DE contigs in shoots, with 170 contigs up- and 272 contigs down-regulated in response to nickel (Figure 1A). This result suggests that nickel accumulation has a more pronounced effect on the shoot transcriptome. However, we could not identify enriched functional categories among DE contigs in shoots. In particular, we did not identify anyDE contigs encoding proteins involved in metal homeostasis.

*IREG/ferroportin genes in Leucocroton havanensis*

IREG/FPN transporters have previously been implicated in nickel tolerance and accumulation in plants (Schaaf *et al.*, 2006; Merlot *et al.*, 2014; Meier *et al.*, 2018; García de la Torre *et al.*,

239    2021). Using *Leucocroton havanensis* transcriptome assemblies, we reconstructed the sequence

240    of IREG/FPN genes expressed in this species. We identified 2 distinct transcripts coding for

241    IREG/ferroportin transporters orthologous to *A. thaliana* AtIREG1 and AtIREG2. These

242    transporters, subsequently named LhavIREG1 and LhavIREG2, belong to the Plaza

243    orthologous group (OG) ORTHO05D005013, which corresponds to group 2 IREG/FPN

244    (Figure 2; Figure S1). We identified a third transporter, LhavIREG3, orthologous to the

245    plastidic (group 1) AtIREG3 transporter and belonging to OG ORTHO05D008050. Analysis

246    of the phylogenetic tree obtained with plant IREG/FPN indicates that LhavIREG1 and

247    LhavIREG2 originated from a duplication of an IREG/FPN ancestral gene in the

248    Euphorbiaceae, independent of the duplication that occurred in the Brassicaceae and gave rise

249    to the paralogous groups represented by AtIREG1 and AtIREG2. It is therefore not possible to

250    infer the function of the *Leucocroton havanensis* IREG/FPN transporters from the known

251    function of AtIREG1 and AtIREG2, which act at the plasma membrane and  vacuole

252    respectively (Schaaf *et al.*, 2006; Morrissey *et al.*, 2009).

253

254    ***Analysis of LhavIREG1 and LhavIREG2 expression in Leucocroton havanensis***

255    We analyzed the expression of *LhavIREG1 and LhavIREG2* in *L. havanensis* by RT-qPCR

256    (Figure 3). This analysis revealed that both genes are expressed at a similar level in shoots but

257    that *LhavIREG1* is more expressed than *LhavIREG2* in roots. These results are supported by

258    the analysis of RNA-Seq data (Table S2). Based on RNA-Seq data, we did not observe a

259    significative effect of nickel on the expression of IREG/FPN genes in *L. havanensis* (Figure 1).

260    These results suggest that both genes are constitutively expressed in *L. havanensis* and that

261    *LhavIREG1* predominantly acts in roots while both genes are likely playing a function in leaves.

262

263    *LhavIREG1 and LhavIREG2 act as nickel exporters*

264    We have previously shown that *LhavIREG2* expression in yeast increases nickel tolerance

265    (García de la Torre *et al.*, 2021). To further characterize the activity of LhavIREG2 and

266    LhavIREG1, we measure nickel accumulation in yeast cells expressing each of these

267    transporters (Figure 4). The expression of both LhavIREG1 and LhavIREG2 reduces nickel

268    accumulation compared to yeast transformed with the control vector. The same result is

269    observed with *A. thaliana* AtIREG2. These results suggest that both LhavIREG1 and

270    LhavIREG2 transport nickel out of yeast cells, which is consistent with the conserved role of

271    IREG/FPN as divalent metal exporters.

272

273    *LhavIREG1 and LhavIREG2 localize to different membranes in plant cells*

274    To analyze the localization of LhavIREG1 and LhavIREG2 in plant cells, we fused the two

275    transporters with the green fluorescent protein (GFP) at the C-terminal end and expressed the

276    fusion proteins in the *A. thaliana ireg2* mutant. Root cells of the transgenic T2 lines were

277    imaged by confocal microscopy (Figure 5). Lines expressing LhavIREG1-GFP show a thin

278    GFP fluorescent signal delineating the periphery of the root cells (Figure 5 A, B). This signal

279    indicates that LhavIREG1 is mainly localized to the plasma membrane. In contrast, the GFP

280    signal associated with the expression of LhavIREG2-GFP outlines large cytoplasmic vesicles,

281    suggesting a vacuolar localization (Figure 5 C, D). These results indicate that LhavIREG1 and

282    LhavIREG2 localize to different membranes and therefore likely have distinct cellular

283    functions.

284

285    *Expression of LhavIREG1 and LhavIREG2 in A. thaliana differentially affects nickel*

286    *sensitivity and accumulation*

13

287    We used the same *ireg2* transgenic lines expressing *LhavIREG1-GFP* and *LhavIREG2-GFP* to

288    study the effect of the ubiquitous expression of these transporters on nickel tolerance and

289    accumulation (Figure 6). As observed in previous works (Schaaf *et al.*, 2006; Merlot *et al.*,

290    2014), the *A. thaliana ireg2* mutant is more sensitive to root growth in the presence of nickel

291    than the wild type (Figure 6A, B, C). Expression of both *LhavIREG1-GFP* and *LhavIREG2-*

292    *GFP* in *ireg2* significantly increases root growth in the presence of 30 µM nickel compared to

293    *ireg2* or the wild-type (Figure 6A, B, C, D). In addition, transgenic lines expressing

294    *LhavIREG1-GFP* and *LhavIREG2-GFP* do not exhibit the chlorotic phenotype observed in

295    *ireg2* leaves in the presence of nickel. Transgenic lines expressing *LhavIREG1-GFP* show a

296    strong tolerance to 50 µM nickel, a concentration that strongly affects the root growth of the

297    other genotypes (Figure 6D).

298    To further characterize these transgenic lines, we measured nickel accumulation in both roots

299    and shoots (Figure 6E, F). The *ireg2* mutant, which is impaired in the vacuolar sequestration of

300    nickel in roots, translocates and accumulates more nickel in shoots (Schaaf *et al.*, 2006; Merlot

301    *et al.*, 2014). Expression of the vacuolar *LhavIREG2* in *ireg2* transgenic lines slightly increases

302    nickel accumulation in roots, but does not restore nickel accumulation as in wild type (p=0.02),

303    indicating a partial complementation of the *ireg2* phenotype. In contrast, expression of

304    *LhavIREG1* further reduces nickel accumulation in roots compared to the *ireg2* mutant

305    (p=0.03). In these experiments, we cannot observe a significant effect of *LhavIREG1-GFP* and

306    *LhavIREG2-GFP* expression on nickel accumulation in leaves compared to *ireg2* (Figure 6F),

307    but plants expressing *LhavIREG1-GFP* accumulate significantly more nickel in leaves than

308    wild type (p=0.02). These results indicate that the ubiquitous expression of both *LhavIREG1*

309    and *LhavIREG2* leads to a large increase in nickel tolerance, albeit through different cellular

310    mechanisms.

311

**Discussion**

In this work, we provided new molecular insights into the mechanisms involved in nickel hyperaccumulation in the Cuban endemic species *Leucocroton havanensis* (Jestrow *et al.*, 2012; González and Matrella, 2013). We generated a novel transcriptome assembly containing genes expressed in roots and shoots in this species (Table 1). Using this assembly as a reference, we examined the expression of genes in response to nickel treatment and thus nickel hyperaccumulation (Fig. 1). Our results indicate that nickel treatment elicits a more complex response in shoots (442 DE genes) than in roots (27 DE genes). Enrichment analysis revealed that genes encoding for seed storage proteins are induced by nickel in roots. The biological significance of this response is unclear. No other functional category, including the regulation of metal homeostasis, is enriched in response to nickel. In recent years, metal transporters of the IREG/FPN family have been identified as candidate genes involved in nickel tolerance and accumulation (Schaaf *et al.*, 2006; Merlot *et al.*, 2014; Meier *et al.*, 2018; García de la Torre *et al.*, 2021). Analysis of the expression of the two genes encoding group 2 IREG/FPN transporters, *LhavIREG1* and *LhavIREG2*, indicates that both genes are significantly expressed in *L. havanensis*, but are not regulated at the transcriptional level by nickel (Fig. 1, 3). These results are in line with a model suggesting that nickel hyperaccumulation at the species level is associated with a high and constitutive expression of genes involved in metal homeostasis and transport (Verbruggen *et al.*, 2009; Krämer, 2010).

We further investigated the putative function of LhavIREG1 and LhavIREG2 in nickel hyperaccumulation. Our data showed that LhavIREG1 and LhavIREG2 are both nickel exporters (Fig. 4), but localize to the plasma membrane and the vacuole, respectively (Fig. 5). The equivalent dual localization was previously observed for *Arabidopsis thaliana* AthaIREG1 and AthaIREG2 (Schaaf *et al.*, 2006; Morrissey *et al.*, 2009). This observation suggests that in these two distant genera, the duplication of an ancestral group 2 IREG/FPN gene resulted in

15

337 two transporters that convergently evolved into a plasma membrane and a vacuolar form. The

338 molecular determinants of the localization of the IREG/FPN transporters are not yet known.

339 Recently, the presence of a dileucine motif [D/E]X$_{3-5}$L[L/I] (Bonifacino and Traub, 2003;

340 Komarova *et al.*, 2012) was shown to be involved in the vacuolar localization of *A. thaliana*

341 NRAMP3 and NRAMP4 transporters (Müdsam *et al.*, 2018). At least three canonical dileucine

342 motifs are found in the large cytoplasmic loop and C-terminal extension of LhavIREG2 but not

343 LhavIREG1 (Fig. S1). Further studies will be required to support the role of these motifs in the

344 vacuolar localization of LhavIREG2.

345 As anticipated, ectopic and constitutive expression of the vacuolar LhavIREG2 increases nickel

346 tolerance in the *A. thaliana ireg2* mutant. Surprisingly, expression of the plasma membrane

347 LhavIREG1 increases nickel tolerance to a greater extent (Fig. 6). Elemental analysis indicates

348 that LhavIREG1 expression further reduces nickel accumulation in roots compared to *ireg2* and

349 simultaneously increases accumulation in shoots. These results suggest that ectopic expression

350 of LhavIREG1 does not drive the export of nickel from root cells, but rather promotes its

351 translocation to the shoots. This proposed function of LhavIREG1 in metal translocation was

352 previously proposed for *A. thaliana* IREG1 (Morrissey *et al.*, 2009). *A. thaliana ireg2* plants

353 expressing LhavIREG1 show no symptoms of nickel toxicity in leaves, suggesting nickel is

354 accumulated in a compartment where it is less toxic. Since LhavIREG1 localizes to the plasma

355 membrane, we propose that nickel is exported out of leaf cells and bound to the cell wall.

356 Further experiments, including elemental imaging, would be required to support this

357 hypothesis. Interestingly, while vacuolar sequestration of nickel is recognized as an essential

358 function for nickel tolerance and hyperaccumulation (Schaaf *et al.*, 2006; Merlot *et al.*, 2014;

359 García de la Torre *et al.*, 2021), nickel is also associated with the cell wall in leaves of several

360 hyperaccumulators (Krämer *et al.*, 2000; Bidwell *et al.*, 2004; van der Ent *et al.*, 2019). Taken

361 together, our data suggest that in addition to vacuolar IREG/Ferroportin transporters, plasma

362    membrane IREG/FPN also play an important role in hyperaccumulation, mediating efficient

363    translocation of nickel from roots to shoots and nickel export from leaf cells to limit its toxicity.

364

**Data and code availability**

The data discussed in this publication have been deposited in NCBI's Gene Expression Omnibus (Edgar *et al.*, 2002) and are accessible through GEO Series accession number GSE237255 (https://www.ncbi.nlm.nih.gov/geo/query/acc.cgi?acc=GSE237255). Previous Leucocroton data (Lhav_v1) are available through GEO GSE116049. *LhavIREG1* and *LhavIREG2* cDNA sequences were deposited to GenBank under OR234317 and OR234318 accession numbers respectively.

**Contributions**

DAG and SM: conceptualization; DAG, VSGT and SM: methodology; DAG, VSGT and SM: formal analysis; DAG, VSGT, RRF, LB and SM: investigation; DAG: resources; VSGT and SM: data curation; DAG and SM: writing - review & editing; DAG, VSGT and SM: visualization; DAG, VSGT and SM: supervision; SM: funding acquisition.

## Bibliography

**Becher M, Talke IN, Krall L, Krämer U**. 2004. Cross-species microarray transcript profiling reveals high constitutive expression of metal homeostasis genes in shoots of the zinc hyperaccumulator Arabidopsis halleri. Plant J **37**, 251–268.

**Bidwell SD, Crawford SA, Woodrow IE, Sommer-Knudsen J, Marshall AT**. 2004. Sub-cellular localization of Ni in the hyperaccumulator, Hybanthus floribundus (Lindley) F. Muell. Plant, Cell and Environment **27**, 705–716.

**Bonifacino JS, Traub LM**. 2003. Signals for Sorting of Transmembrane Proteins to Endosomes and Lysosomes. Annual Review of Biochemistry **72**, 395–447.

**Conte S, Stevenson D, Furner I, Lloyd A**. 2009. Multiple antibiotic resistance in Arabidopsis is conferred by mutations in a chloroplast-localized transport protein. Plant physiology **151**, 559–573.

**Corzo Remigio A, Chaney RL, Baker AJM, Edraki M, Erskine PD, Echevarria G, van der Ent A**. 2020. Phytoextraction of high value elements and contaminants from mining and mineral wastes: opportunities and limitations. Plant and Soil **449**, 11–37.

**Craciun AR, Meyer C-L, Chen J, Roosens N, De Groodt R, Hilson P, Verbruggen N**. 2012. Variation in HMA4 gene copy number and expression among Noccaea caerulescens populations presenting different levels of Cd tolerance and accumulation. Journal of Experimental Botany **63**, 4179–4189.

**DalCorso G, Fasani E, Manara A, Visioli G, Furini A**. 2019. Heavy Metal Pollutions: State of the Art and Innovation in Phytoremediation. International Journal of Molecular Sciences **20**, 3412.

**Dudka S, Adriano DC**. 1997. Environmental Impacts of Metal Ore Mining and Processing: A Review. Journal of Environmental Quality **26**, 590–602.

**Edgar RC**. 2004. MUSCLE: multiple sequence alignment with high accuracy and high

throughput. Nucleic Acids Research **32**, 1792–1797.

**Edgar R, Domrachev M, Lash AE**. 2002. Gene Expression Omnibus: NCBI gene expression and hybridization array data repository. Nucleic Acids Research **30**, 207–210.

**van der Ent A, Baker AJM, Reeves RD, *et al.*** 2015. Agromining: Farming for Metals in the Future? Environmental Science & Technology **49**, 4773–4780.

**van der Ent A, Baker AJM, Reeves RD, Pollard AJ, Schat H**. 2013. Hyperaccumulators of metal and metalloid trace elements: Facts and fiction. Plant and Soil **362**, 319–334.

**van der Ent A, Spiers KM, Brueckner D, Echevarria G, Aarts MGM, Montargès-Pelletier E**. 2019. Spatially-resolved localization and chemical speciation of nickel and zinc in Noccaea tymphaea and Bornmuellera emarginata. Metallomics **11**, 2052–2065.

**Escudero V, Abreu I, Tejada-Jiménez M, *et al.*** 2020. Medicago truncatula Ferroportin2 mediates iron import into nodule symbiosomes. New Phytologist **228**, 194–209.

**García de la Torre VS, Majorel-Loulergue C, Rigaill GJ, *et al.*** 2021. Wide cross-species RNA-Seq comparison reveals convergent molecular mechanisms involved in nickel hyperaccumulation across dicotyledons. New Phytologist **229**, 994–1006.

**González DA, Matrella S**. 2013. Nickel hyperaccumulation 'in vitro' by Leucocroton havanensis (Euphorbiaceae) / Hiperacumulación 'in vitro' de Ni en Leucocroton havanensis (Euphorbiaceae). Revista del Jardín Botánico Nacional **34/35**, 83–88.

**Halimaa P, Lin Y-F, Ahonen VH, *et al.*** 2014. Gene expression differences between Noccaea caerulescens ecotypes help to identify candidate genes for metal phytoremediation. Environmental science & technology **48**, 3344–53.

**Hammond JP, Bowen HC, White PJ, Mills V, Pyke KA, Baker AJM, Whiting SN, May ST, Broadley MR**. 2006. A comparison of the Thlaspi caerulescens and Thlaspi arvense shoot transcriptomes. New Phytologist **170**, 239–260.

**Hanikenne M, Talke IN, Haydon MJ, Lanz C, Nolte A, Motte P, Kroymann J, Weigel D,**

**Krämer U**. 2008. Evolution of metal hyperaccumulation required cis-regulatory changes and triplication of HMA4. Nature **453**, 391–395.

**Jestrow B, Gutiérrez Amaro J, Francisco-Ortega J**. 2012. Islands within islands: a molecular phylogenetic study of the Leucocroton alliance (Euphorbiaceae) across the Caribbean Islands and within the serpentinite archipelago of Cuba. Journal of Biogeography **39**, 452–464.

**Kan M, Fujiwara T, Kamiya T**. 2022. Golgi-Localized OsFPN1 is Involved in Co and Ni Transport and Their Detoxification in Rice. Rice **15**, 36.

**Kim LJ, Tsuyuki KM, Hu F, *et al.*** 2021. Ferroportin 3 is a dual-targeted mitochondrial/chloroplast iron exporter necessary for iron homeostasis in Arabidopsis. The Plant Journal **107**, 215–236.

**Komarova NY, Meier S, Meier A, Grotemeyer MS, Rentsch D**. 2012. Determinants for Arabidopsis Peptide Transporter Targeting to the Tonoplast or Plasma Membrane. Traffic **13**, 1090–1105.

**Krämer U**. 2010. Metal Hyperaccumulation in Plants. Annual Review of Plant Biology **61**, 517–534.

**Krämer U, Pickering IJ, Prince RC, Raskin I, Salt DE**. 2000. Subcellular Localization and Speciation of Nickel in Hyperaccumulator and Non-Accumulator Thlaspi Species. Plant Physiology **122**, 1343–1354.

**Letunic I, Bork P**. 2021. Interactive Tree Of Life (iTOL) v5: an online tool for phylogenetic tree display and annotation. Nucleic Acids Research **49**, W293–W296.

**Li Z, Ma Z, van der Kuijp TJ, Yuan Z, Huang L**. 2014. A review of soil heavy metal pollution from mines in China: Pollution and health risk assessment. Science of The Total Environment **468**–**469**, 843–853.

**Lord SJ, Velle KB, Mullins RD, Fritz-Laylin LK**. 2020. SuperPlots: Communicating

21

bioRxiv preprint doi: https://doi.org/10.1101/2023.08.11.552958; this version posted August 11, 2023. The copyright holder for this preprint (which was not certified by peer review) is the author/funder, who has granted bioRxiv a license to display the preprint in perpetuity. It is made available under aCC-BY-NC-ND 4.0 International license.

reproducibility and variability in cell biology. Journal of Cell Biology **219**.

**Manara A, Fasani E, Furini A, DalCorso G**. 2020. Evolution of the metal hyperaccumulation and hypertolerance traits. Plant, Cell & Environment **43**, 2969–2986.

**Meier SK, Adams N, Wolf M, Balkwill K, Muasya AM, Gehring CA, Bishop JM, Ingle RA**. 2018. Comparative RNA-seq analysis of nickel hyperaccumulating and non-accumulating populations of *Senecio coronatus* (Asteraceae). The Plant Journal **95**, 1023–1038.

**Merlot S, Hannibal L, Martins S, Martinelli L, Amir H, Lebrun M, Thomine S**. 2014. The metal transporter PgIREG1 from the hyperaccumulator Psychotria gabriellae is a candidate gene for nickel tolerance and accumulation. J Exp Bot **65**, 1551–1564.

**Morrissey J, Baxter IR, Lee J, Li L, Lahner B, Grotz N, Kaplan J, Salt DE, Guerinot M Lou**. 2009. The Ferroportin Metal Efflux Proteins Function in Iron and Cobalt Homeostasis in Arabidopsis. The Plant Cell **21**, 3326–3338.

**Müdsam C, Wollschläger P, Sauer N, Schneider S**. 2018. Sorting of Arabidopsis NRAMP3 and NRAMP4 depends on adaptor protein complex AP4 and a dileucine-based motif. Traffic **19**, 503–521.

**Ó Lochlainn S, Bowen HC, Fray RG, Hammond JP, King GJ, White PJ, Graham NS, Broadley MR**. 2011. Tandem Quadruplication of HMA4 in the Zinc (Zn) and Cadmium (Cd) Hyperaccumulator Noccaea caerulescens (I Baxter, Ed.). PLoS ONE **6**, e17814.

**Oomen RJFJ, Wu J, Lelièvre F, Blanchet S, Richaud P, Barbier-Brygoo H, Aarts MGM, Thomine S**. 2009. Functional characterization of NRAMP3 and NRAMP4 from the metal hyperaccumulator Thlaspi caerulescens. New Phytologist **181**, 637–650.

**Pfaffl MW**. 2001. A new mathematical model for relative quantification in real-time RT-PCR. Nucleic Acid Research **29**, 16–21.

**Reeves RD, Baker AJM, Jaffré T, Erskine PD, Echevarria G, Ent A**. 2018. A global

22

database for plants that hyperaccumulate metal and metalloid trace elements. New Phytologist **218**, 407–411.

**Schaaf G, Honsbein A, Meda AR, Kirchner S, Wipf D, von Wirén N**. 2006. AtIREG2 Encodes a Tonoplast Transport Protein Involved in Iron-dependent Nickel Detoxification in Arabidopsis thaliana Roots. Journal of Biological Chemistry **281**, 25532–25540.

**Seppey M, Manni M, Zdobnov EM**. 2019. BUSCO: Assessing Genome Assembly and Annotation Completeness BT - Gene Prediction: Methods and Protocols. In: Kollmar M, ed. New York, NY: Springer New York, 227–245.

**Smith-Unna R, Boursnell C, Patro R, Hibberd J, Kelly S**. 2016. TransRate: reference free quality assessment of de novo transcriptome assemblies. Genome Research **26**, 1134–1144.

**Sonter LJ, Dade MC, Watson JEM, Valenta RK**. 2020. Renewable energy production will exacerbate mining threats to biodiversity. Nature Communications **11**, 6–11.

**Suman J, Uhlik O, Viktorova J, Macek T**. 2018. Phytoextraction of Heavy Metals: A Promising Tool for Clean-Up of Polluted Environment? Frontiers in Plant Science **9**, 1–15.

**Taniguchi R, Kato HE, Font J, Deshpande CN, Wada M, Ito K, Ishitani R, Jormakka M, Nureki O**. 2015. Outward- and inward-facing structures of a putative bacterial transition-metal transporter with homology to ferroportin. Nature Communications **6**, 1–10.

**Verbruggen N, Hermans C, Schat H**. 2009. Molecular mechanisms of metal hyperaccumulation in plants. New Phytol **181**, 759–776.

**Vidal O, Le Boulzec H, Andrieu B, Verzier F**. 2022. Modelling the demand and access of mineral resources in a changing world. Sustainability (Switzerland) **14**, 1–16.

**Weber M, Harada E, Vess C, Roepenack-Lahaye E V, Clemens S**. 2004. Comparative microarray analysis of Arabidopsis thaliana and Arabidopsis halleri roots identifies nicotianamine synthase, a ZIP transporter and other genes as potential metal hyperaccumulation factors. The Plant Journal **37**, 269–281.

**Table 1** : Parameters of *Leucocroton havanensis* transcriptome assembly (Lhav_v2)

| **Contig metrics** | |
|---|---|
| Number of contigs | 65936 |
| Number over 1kb | 14320 |
| Mean length (kb) | 757 |
| N50 (kb) | 1196 |
| **Read mapping metrics** | |
| Fragment mapped (%) | 87 |
| Good mapping (%) | 76 |
| **Transrate score** | **0.34** |
| Good contigs (%) | 95 |
| **Busco score (%)** | **69.6** |
| S: 68.7%, D: 0.9%, F: 25.2%, M: 6.1% | |
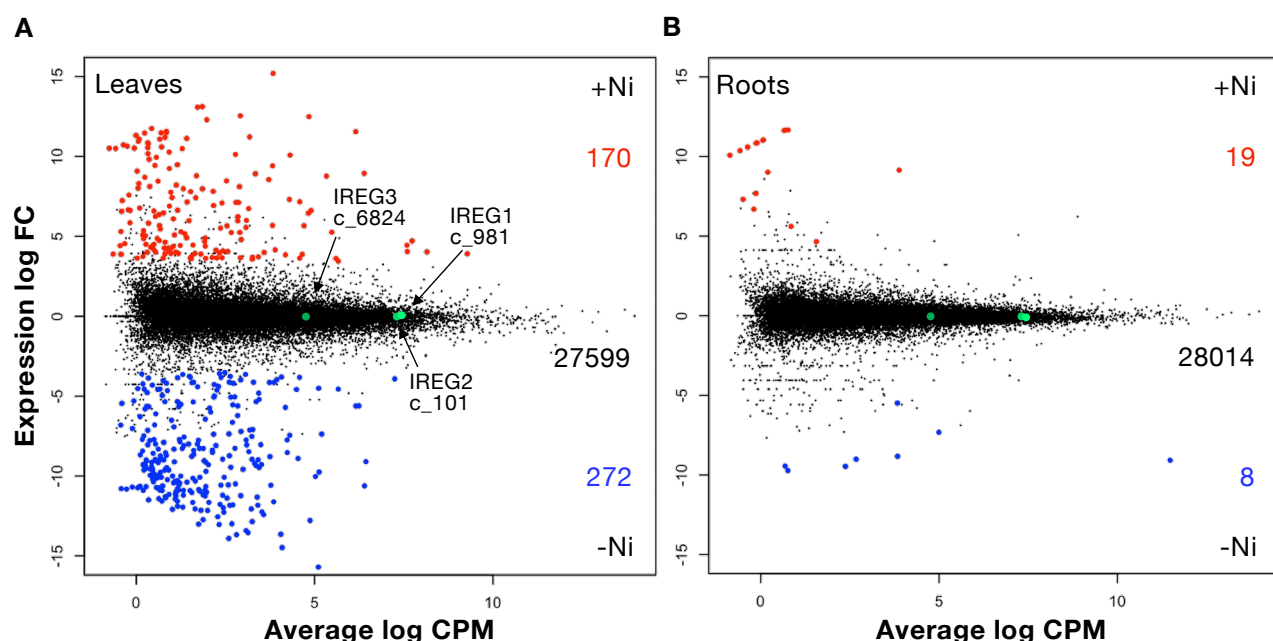
**Fig. 1. Differential gene expression analysis in *Leucocroton havanensis* in response to nickel.** MA plot showing comparative analysis in shoots (A) and roots (B) in the presence (+Ni) or absence (-Ni) of nickel using the Lhav_v2 transcriptome as reference. DE contigs up-regulated in response to nickel or the absence of nickel are colored in red and blue, respectively. Non DE contigs are colored in black. The number of contigs in each category is given on the right side of the panel. The positions of *LhavIREG1* (c_981), *LhavIREG2* (c_101) and *LhavIREG3* (c_6824) are marked with green dots. FC: fold change; CPM: counts per million.
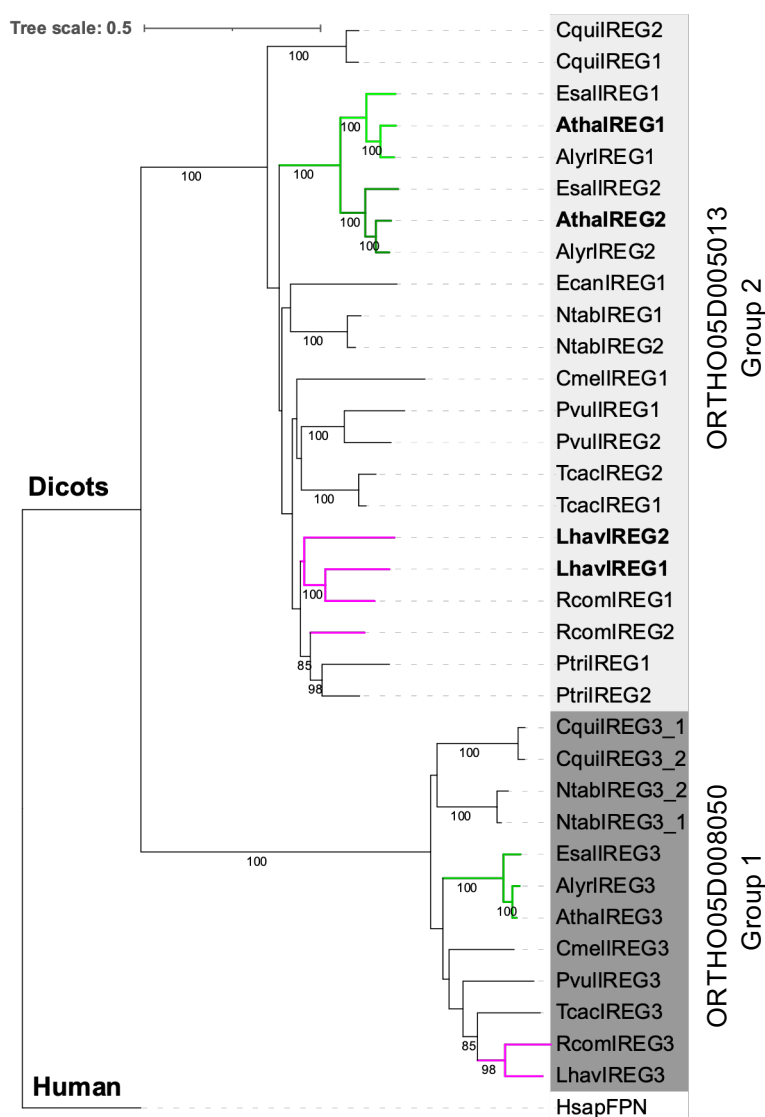
**Fig.2. Phylogenetic tree of the IREG/FPN metal transporter family from Eudicots.** This tree includes IREG/FPN proteins from *Arabidopsis thaliana* (Atha, Brassicaceae), *A. lyrata* (Alyr, Brassicaceae), *Eutrema salsugineum* (Esal, Brassicaceae), *Teobroma cacao* (Tcac, Malvaceae), *Cucumis melo* (Cmel, Cucurbitaceae), *Phaseolus vulgaris* (Pvul, Fabaceae), *Nicotiana tabacum* (Ntab, Solanaceae), *Chenopodium quinoa* (Cqui, Amaranthaceae), *Erigeron canadensis* (Ecan, Asteraceae), *Ricinus communis* (Rcom, Euphorbiaceae), *Leucocroton havanensis* (Lhav, Euphorbiaceae). *Homo sapiens* (Hsap) ferroportin was used as an outgroup. Orthogroups ORTHO05D005013 and ORTHO05D008050 from Plaza 5 are shaded in light and dark gray, respectively. Clades containing Brassicaceae (green) and Euphorbiaceae (magenta) species are highlighted.
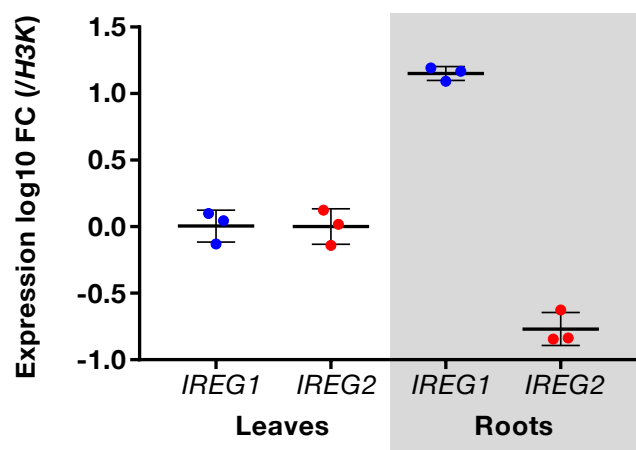
**Fig. 3.** Analysis of the expression of *LhavIREG1* and *LhavIREG2* in leaves and roots. Gene expression measured by RT-qPCR is expressed as log10 fold change (FC) compared to *H3K* expression. Data are mean value ± SD (n=3 independent samples).
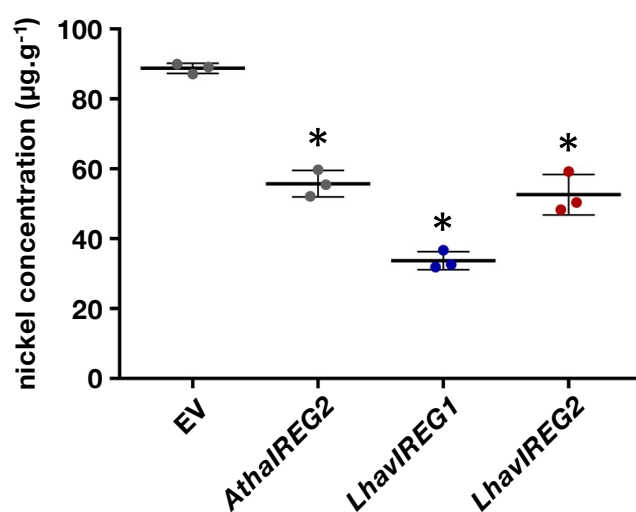
**Fig. 4: Nickel accumulation in yeast cells expressing *LhavIREG1* and *LhavIREG2*.** Nickel concentration was measured by MP-AES in yeast cells expressing *LhavIREG1, LhavIREG2* and *AthaIREG2* or transformed with pDR195 (EV). For each construct, the results are mean value ± SD (n = 3; independent transformants). * $p < 0.01$ (Welch's t-test), comparedwith EV condition
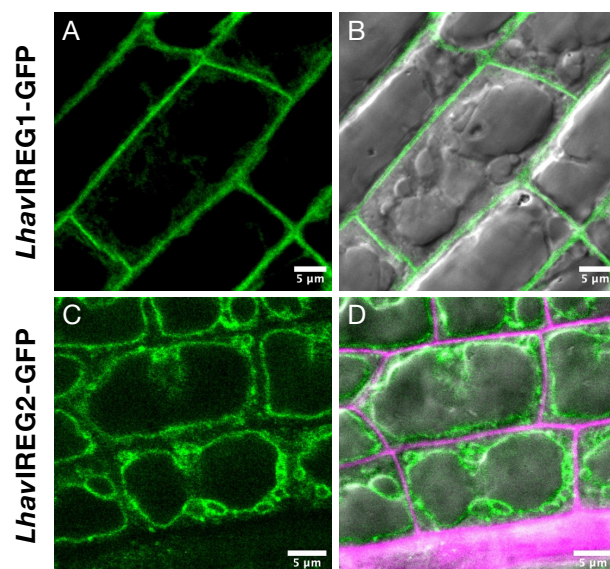
**Fig. 5. Localization of *Lhav*IREG1 and *Lhav*IREG2 in plant cells.** Root cells of *A. thaliana ireg2* mutant stably expressing *Lhav*IREG1-GFP (A, B) and *Lhav*IREG2-GFP (C, D) were imaged by confocal microscopy. GFP-associated fluorescence is shown in green (A, C). Corresponding composite images with DIC images are also shown (B, D). Propidium iodine Cell walls labelled with are shown in magenta. Scale bars are 5 μm.
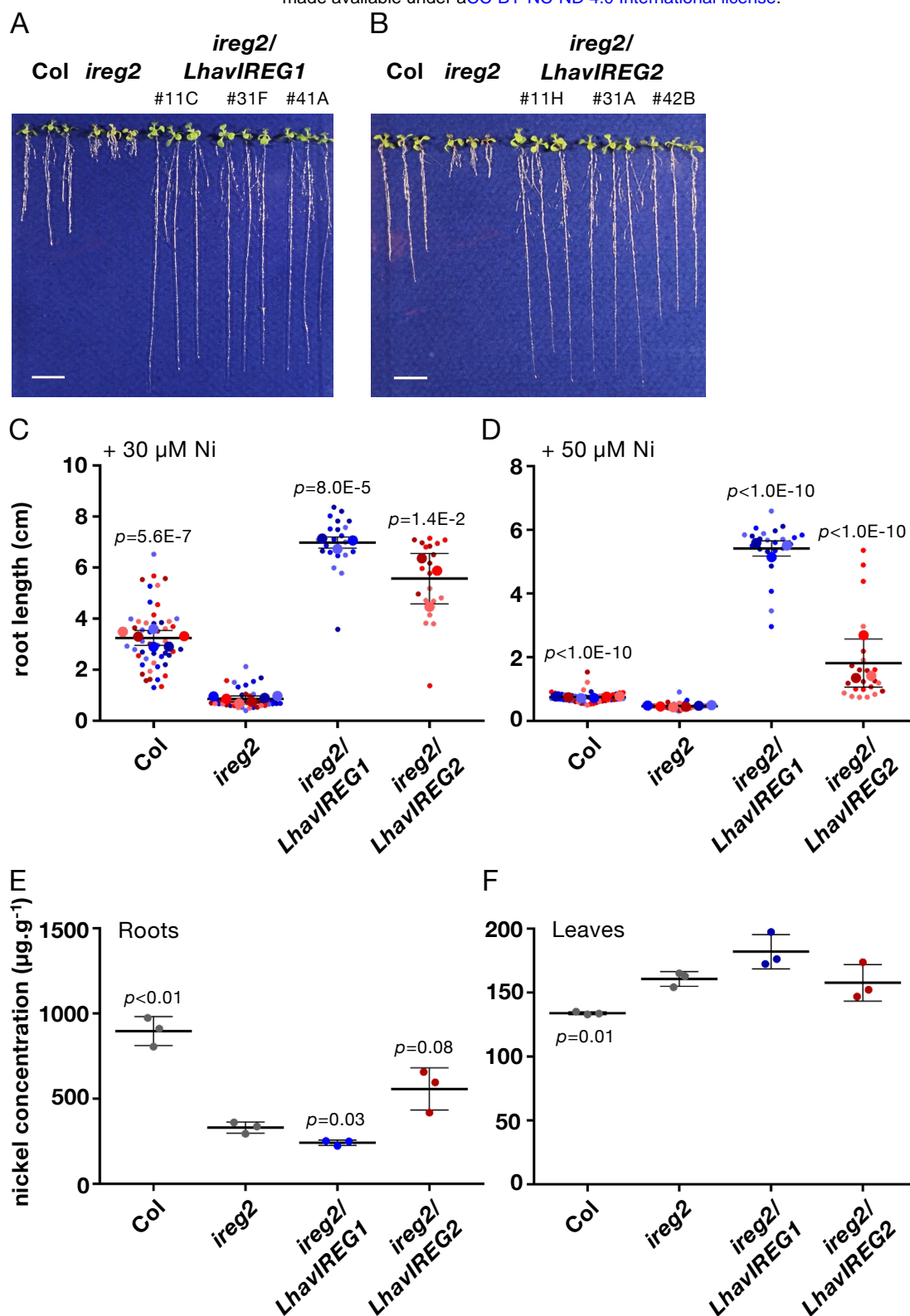
**Fig. 6. Effect of LhavIREG1 and LhavIREG2 expression on nickel tolerance and accumulation.** Pictures of individual *A. thaliana ireg2* transgenic lines expressing *LhavIREG1-GFP* (A) and *LhavIREG2-GFP* (B) grown on a culture medium containing 30 μM $NiCl_2$ for 10 days together with wild type (Col) and the *ireg2* mutant. Three representative plantlets were selected per line. Scale bars correspond to 1 cm. (C) Quantification of root growth of plantlets grown in the presence of 30 μM $NiCl_2$ and (D) 50 μM $NiCl_2$. Each small dot represents an individual measurement. Large dots represent the mean value for each individual line or experiment. Means (n=3 independent transgenic lines, n=6 for Col and *ireg2*) ± SEM are shown. *p*-values were calculated compared to *ireg2*. Nickel concentrations were measured in roots (E) and leaves (F) of the same genotypes. Data are mean value ± SD (n=3 independent transgenic lines or experiments). *p*-values were calculated relative to *ireg2*.